Electron-impact dissociation of ozone cations to O^+ fragments

D. S. Belic,[1,*] X. Urbain,[2] and P. Defrance[2]

[1]*Faculty of Physics, University of Belgrade, PO Box 386, 11000 Belgrade, Serbia*

[2]*Institute of Condensed Matter and Nanosciences, Université Catholique de Louvain, Louvain-la-Neuve B-1348, Belgium*

(Received 17 November 2014; published 8 January 2015)

Absolute cross sections for electron-impact dissociation of O_3^+ ions yielding an O^+ fragment are measured. The animated electron-ion crossed-beam method is applied in the energy range from 1 eV to 2.5 keV. The maximum total cross section for O^+ fragment production is found to be $(3.6 \pm 0.3) \times 10^{-16}$ cm^2 at 75 eV and such a large value of the cross section extends down to low energies. The threshold energy is found to be below 2 eV. Contributions of dissociative excitation and dissociative ionization to O^+ fragment production are determined separately. The total kinetic energy release distributions are determined at select electron energies. Present data are discussed and compared with recent results [S. H. M. Deng *et al.*, Phys. Rev. A **82**, 062715 (2010)].

DOI: 10.1103/PhysRevA.91.012703 PACS number(s): 34.80.Ht

I. INTRODUCTION

Ozone plays an important role in the terrestrial atmosphere, both in the troposphere and in the stratosphere. In particular, the stratospheric ozone layer absorbs energetic ultraviolet light that is responsible for some human tissue and immune system damage on earth [1]. In relation to the stratospheric layer depletion problem, ozone has been extensively studied in the past few decades. After the discovery of the Antarctic ozone hole [2,3], intensive research has focused on the study of various destruction mechanisms of the ozone molecule and the ozone cation.

It has been recognized and explained that ozone decomposes by absorbing UV radiation or by reactions with radicals of nitric oxides or water molecules. Ozone is also depleted efficiently by chlorine and bromine atoms or oxides, which act as catalysts for ozone consumption processes [4]. These species come mainly from air pollutants, such as the chlorofluorocarbon and bromofluorocarbon (halon) compounds, which have small concentrations but long lifetimes in the stratosphere. Furthermore, the reactions of the ozone molecule and the ozone cation with charged particles, e.g., with ions and with electrons, can contribute to the destruction of the ozone layer as well.

The first measurements of electron-impact vibrational excitation of ozone were published by Davies *et al.* [5]. Evidence was given for the formation of a low-lying shape resonance at approximately 4 eV. Attachment of electrons with energies of 1.2–2 eV to ozone was found to lead to vibrationally excited O_2^-, which subsequently loses electrons by vibrational autodetachment [6]. The absolute integral cross section for this process was found to be substantial and permits an independent determination of the dissociation energy of ozone of 1.06 eV.

Absolute differential cross-section measurements, conducted by means of a crossed-beam technique, of inelastic electron impact on ozone were published by Sweeney and Shyn [7] for excitation of the Hartley band. Lying between about 4 and 6 eV in excitation energy, this band is the one most crucial for the filtering of ultraviolet radiation in the atmosphere. Furthermore, its excitation results in the dissociation of ozone into chemically reactive fragments. The impact energies employed were 7, 10, 15, and 20 eV. The angular dependence of the cross sections, from 12° to 156°, indicates the presence of at least one forbidden transition, in addition to the well known $1\,^1B_2 \leftarrow X\,^1A_1$ allowed transition present in optical spectra.

Electron-impact ionization of ozone has been studied both experimentally and theoretically. Experimental results were published by Siegel [8] and by Newson *et al.* [9] in the energy region from threshold to 500 eV. The maximum of the cross section was found in both cases to be $(2.4 \pm 0.4) \times 10^{-16}$ cm^2 at 100 eV and the threshold energy was extrapolated to 16 eV. Theoretical binary-encounter Bethe results of Kim *et al.* [10] are about 60% higher than the experimental values over the entire energy range [8,9]. They have determined the threshold energy to be (13.2 ± 0.5) eV. The data of Newson *et al.* [9] are renormalized by the NIST Standard Reference Database [11] to be $(3.8 \pm 0.5) \times 10^{-16}$ cm^2 at 100 eV.

The ozone cation O_3^+ exists naturally in the atmosphere and is important for our understanding of ozone depletion as well [12]. The theoretical calculation of the electronic states of the ozone cation is difficult due to strong electron correlation and there are details of potential energy surfaces that are lacking.

The O_3^+ ion is nonlinear and the bond distance and angle differ significantly for each electronic state. The first photoelectron spectra of O_3^+ were obtained by Frost *et al.* [13], but the assignment of the states was not clarified until Willitsch *et al.* [14]. The three lowest doublet states of O_3^+ are assigned as $X\,^2A_1$, $A\,^2B_2$, and $B\,^2A_2$ and their energies are all within 1 eV apart. The calculation of Speakman *et al.* [15] shows that the three lower quartet states are also close in energy, lying up to 2 eV above the ground state of O_3^+. The ozone cation is weakly bound and easily dissociates by photon absorption, electron collision, or recombination.

Electron-impact dissociative recombination of O_3^+ has been investigated by the ion storage-ring method [16] and is dominated at 0 eV by three-body dissociation. The photodissociation of O_3^+ yielding O^+ or O_2^+ fragments has also been studied intensively. Vestal and Mauclaire [17] reported that the cross section of the O^+ channel is predominant in the visible range.

*belicd@ff.bg.ac.rs

More recently, absolute cross sections for electron-impact dissociation of O_3^+ ions yielding O^+ and O_2^+ fragment ions have been measured by Deng *et al.* [18]. An electron-ion crossed-beam method has been used for energies from about 3 to 100 eV. While the O_2^+ channel dominates the dissociation cross section over the measured energy range, a strong enhancement is also observed in the O^+ channel at low energy.

Species of interest for the astrophysical and plasma physics community for low-energy discharges as well as for the fusion plasma are currently investigated in our laboratory. Particular attention is devoted to the constituents of the earth's atmosphere and to air pollutants that are emitted in the environment. A crossed-beam experimental setup designed to measure electron-impact cross sections of molecular ions is used for this purpose. Electron-impact ionization of CO_2^+ [19] and ionization and dissociation of CO^+ and some hydrocarbons [20,21] have been studied in detail. Similar experiments with O_2^+ and D_3^+, linked to the present work, were also carried out [22,23].

In the present work, we report the measured absolute cross sections for electron-impact dissociation of O_3^+ producing O^+ fragments. Possible channels leading to O^+ ions include the following reactions:

$$e^- + O_3^+ \rightarrow e^- + O^+ + O_2 \quad (2.19\ \text{eV}) \tag{1}$$

$$\rightarrow e^- + O^+ + O + O \quad (7.35\ \text{eV}) \tag{2}$$

$$\rightarrow 2e^- + O^+ + O_2^+ \quad (14.26\ \text{eV}) \tag{3}$$

$$\rightarrow 2e^- + O^+ + O^+ + O \quad (20.97\ \text{eV}), \tag{4}$$

where the energies given in parentheses are the threshold for each channel from the $^2A_1$ ground state of O_3^+ [24]. The first two channels are dissociative excitation (DE) processes and the remaining channels are dissociative ionization (DI) processes. Resonant ion-pair formation may also contribute to the measurement of ion fragments, but according to the arguments given by [18], its contribution is expected to be negligible.

The experimental setup, measurement procedure, and data analysis method are described hereafter. They allow us to (i) measure the absolute cross sections for O^+ ion production, (ii) estimate partial contributions from DE and DI separately, and (iii) determine the total kinetic energy release distributions. The present results are compared with existing data from the literature.

II. EXPERIMENTAL PROCEDURE

In this experiment, the animated electron-ion crossed-beam technique is used [25]. It has been described in detail elsewhere [20] and only a brief outlook will be given here. The molecular ion beam is produced in an electron cyclotron resonance (ECR) ion source by the introduction of oxygen. The ions are produced at low microwave power, less than 1 W, injected in the source. The source operates at a gas pressure higher than 3×10^{-2} Torr. Even under these favorable conditions the beam current is typically 0.2 nA. The O_3^+ ion beam is accelerated to 8 keV and crossed at right angles with the electron beam. Product ions are separated from the primary ion beam by using a double focusing 90° magnetic analyzer and deflected by a 90° electrostatic spherical deflector onto the channel electron multiplier.

In the animated electron-ion beam method, the electron beam is swept across the ion beam in a linear motion at a constant speed u. The total number of events K produced during one complete passage of the electrons through the ion beam is related to the measured cross section σ_m by

$$\sigma_m = \frac{uK}{I_e I_i \gamma} \frac{v_e v_i q_i e^2}{\left(v_e^2 + v_i^2\right)^{1/2}}. \tag{5}$$

In this expression, γ is the detector efficiency and I_e and I_i, e and $q_i e$, and v_e and v_i are the electron-beam and ion-beam current intensities, the charges, and the velocities of the electrons and ions, respectively.

The measurements are performed at collision energies from 1 to 2500 eV. Electron energies are calibrated by the Ne^+ ionization threshold and corrected for the contact potentials. The uncertainty of the collision energy is estimated to be 0.5 eV.

Due to transfer of internal energy to kinetic energy of the fragments, dissociation products exhibit both a broad velocity and a broad angular distribution in the laboratory frame. The angular acceptance of the magnetic analyzer generally allows total transmission of the fragments. However, fragment velocity dispersion in the magnetic analyzer usually exceeds the detector acceptance, limited by its actual size. This results in a partial loss of the signal. In order to compensate for this effect, careful magnetic-field scans of the signal have been performed at select electron energies.

In a separate test, electron-impact single ionization of ions has been used to determine the detector analyzer acceptance, e.g., the transmission efficiency η of the experiment. Single-ionization products have a narrow velocity distribution, the same as the primary beam. In other words, the product ion velocity is not affected by the dissociation. Thus, by performing analyzer magnetic-field scans for these ions, one can find the range of the field ΔB, from which the ions are detected. The rest of the spectrum outside this region is lost. The ratio $\Delta B/B_0$ is found to be 0.007 for the actual experimental setup.

In order to put the cross section on an absolute scale, the apparent cross section $\sigma_m(B)$ is first measured at a given electron energy as a function of the analyzer magnetic field B. Next the velocity distribution spectrum is computed from this apparent cross-section scan and the total cross section σ is obtained by integrating this distribution over the entire velocity range. The transmission efficiency of the experiment η, determined as the ratio of the apparent cross section $\sigma_m(B)$ to the total cross section σ, is obtained for several energies and extrapolated over the entire electron energy range. This efficiency is used to calculate absolute cross sections.

The shape of the fragment velocity distributions depends on the electron energy, i.e., on the various channels involved in the reaction. At low energies, i.e., below the ionization threshold, only DE is observed. The width of the spectrum increases with increasing electron energy. The spectra become significantly broader at high electron energies due to Coulomb repulsion experienced by the charged fragments produced by DI of the parent ions. The spectra taken above the ionization threshold

therefore exhibit two contributions that indicate the presence of two distinct dissociative contributions: A narrower part of the distribution that corresponds to DE is superimposed on a wider part that originates from the DI process. Consequently, the pure DI contribution can be obtained by fitting the outer wider part of the spectrum. Subtraction of this contribution from the total signal leads to the DE part of the spectrum. In this way, the contributions of DE and DI can be separated and corresponding absolute cross sections σ_{DE} and σ_{DI} can be inferred.

Furthermore, the total kinetic energy release (KER) distribution of the investigated fragments can be expressed in terms of the velocity distributions [20]. The total kinetic energy release distribution for the investigated process is expressed in terms of the velocity distribution by

$$\frac{d\sigma(E_{KER})}{dE_{KER}} = \frac{-2\mu v_c}{m^2}\frac{d}{dv}\left[\frac{1}{v}\frac{d\sigma(v)}{dv}\right]. \quad (6)$$

Here m is the fragment ion mass, μ is the reduced mass of the fragments, v_c represents the center-of-mass velocity, and E_{KER} represents the sum of the kinetic energy released to the dissociation fragments.

The dominant contributions to the systematic uncertainties in the experiment come from the beam sweeping velocity measurement (1%), ion and electron current measurements (0.5%), and detection efficiency (1%) at a level equivalent to a 90% confidence level for statistical uncertainties. Additional uncertainty is introduced by the transmission efficiency η, of the order of 8%. This gives, in a quadrature sum, a total absolute cross-section uncertainty of $\pm 10\%$. Another uncertainty is introduced by the DE and DI separation procedure and we have estimated uncertainties for σ_{DE} and σ_{DI} to be $\pm 15\%$. The uncertainty associated with the electron energy is estimated to be ± 0.5 eV. The pressure is kept below 1×10^{-9} mbar in the collision chamber during the measurement in order to reduce the background.

III. RESULTS AND DISCUSSION

Absolute cross sections for electron-impact dissociation of O_3^+ producing O^+ fragment ions are presented for energies up to 2500 eV. First, at select electron energies, magnetic-field scans of the apparent cross sections are measured. These scans are shown in Fig. 1 for energies of 15, 25, 95, and 295 eV. All scans are centered at 111 mT, which corresponds to the unaffected fragment ion velocity, but their widths increase significantly with increasing electron energy. This is a consequence of the dissociation energy transferred to the kinetic energy of fragments, as discussed in Sec. II. For electron energies above the ionization threshold, a complex structure of the scans can be seen showing DE and DI contributions. The range ΔB for the current experiment is labeled in Fig. 1 by the two vertical lines (at 110.6 and 111.4 mT). Values obtained for η as discussed above are extrapolated over the whole electron energy region and they range from 100% at threshold to some 23% at high energy. The ratio of the measured cross section and corresponding transmission factor gives the absolute total cross section for a given electron energy. The results of the absolute cross section for electron-impact dissociation of O_3^+ producing O^+

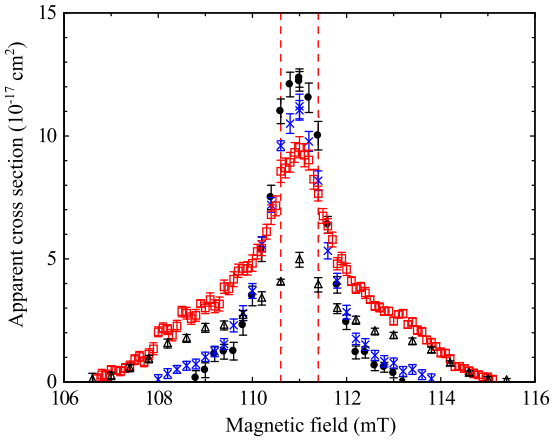

FIG. 1. (Color online) Measured cross sections for O^+ production by electron impact on O_3^+ versus analyzer magnetic field. Electron energies are 15 eV (closed circles), 25 eV (crosses), 95 eV (open squares), and 295 eV (open triangles). The vertical dashed lines indicate the acceptance window ΔB (see the text).

fragment are shown in Fig. 2 and also are listed in Table I, together with the absolute error bars.

The maximum of the cross section is found to be $(3.6 \pm 0.3) \times 10^{-16}$ cm^2 at 75 eV. Such large values of the cross section extend down to low electron energies, with another local maximum of $(3.4 \pm 0.2) \times 10^{-16}$ cm^2 at 6.1 eV. The threshold energy is estimated to be (1.5 ± 0.5) eV. This low-energy threshold indicates that a fraction of the primary ions may be excited, having in mind a number of low-lying metastable levels in O_3^+. The limited energy resolution does not give access to the degree of excitation of the reactants, which may be estimated, however, with the help of thermodynamical considerations. The ozone cation is bound by 0.607 eV as determined by Willitsch *et al.* [14]. A quick estimate of the maximum internal temperature, considering that $\frac{9}{2}k_BT < D_0$, gives 1560 K. However, by analogy with H_3^+, which is

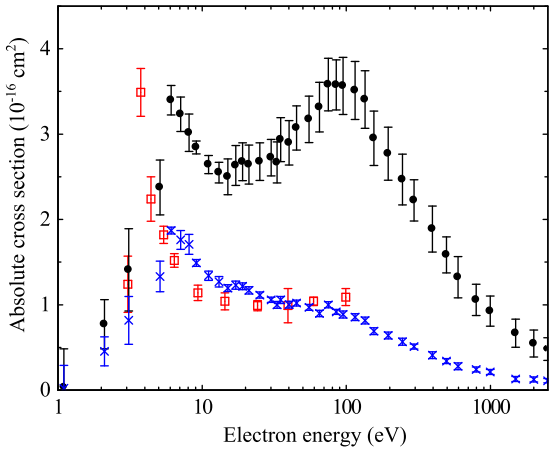

FIG. 2. (Color online) Cross sections for electron-impact dissociation of O_3^+ producing O^+ fragment ions. Closed circles are present data, open squares are data of Deng *et al.* [18], and crosses are present measurements prior to their correction for transmission efficiency (see the text).

TABLE I. Absolute cross sections for total (inclusive) O^+ production, DE, and DI, together with the respective error bars (in 10^{-16} cm^2).

E (eV)	σ_{tot}	$\Delta\sigma_{tot}$	σ_{DE}	$\Delta\sigma_{DE}$	σ_{DI}	$\Delta\sigma_{DI}$
1.1	0.03	0.45	0.03	0.45		
2.1	0.77	0.29	0.77	0.29		
3.1	1.41	0.48	1.41	0.48		
5.1	2.38	0.32	2.38	0.32		
6.1	3.40	0.17	3.40	0.17		
7.1	3.23	0.20	3.23	0.20		
8.1	3.02	0.22	3.02	0.22		
9.1	2.84	0.08	2.84	0.08		
11.1	2.64	0.11	2.64	0.11		
13.1	2.55	0.12	2.55	0.12		
15.1	2.50	0.21	2.49	0.21	0.01	0.04
17.1	2.63	0.23	2.41	0.23	0.22	0.05
19.1	2.68	0.22	2.33	0.22	0.34	0.06
21.1	2.64	0.23	2.20	0.23	0.45	0.07
25.1	2.68	0.22	2.15	0.22	0.53	0.08
30.1	2.72	0.21	1.89	0.21	0.83	0.10
33.1	2.67	0.24	1.68	0.24	1.00	0.10
35.1	2.93	0.26	1.67	0.26	1.27	0.12
40.1	2.90	0.26	1.28	0.26	1.62	0.11
45.1	3.07	0.26	1.27	0.26	1.81	0.30
55.1	3.17	0.27	1.11	0.27	2.06	0.33
65.1	3.32	0.291	0.94	0.29	2.37	0.35
75.1	3.58	0.31	1.04	0.31	2.54	0.37
85.1	3.58	0.29	0.99	0.29	2.59	0.36
95.1	3.56	0.33	0.80	0.33	2.77	0.36
115.1	3.51	0.34	0.84	0.34	2.67	0.34
135.1	3.41	0.34	0.85	0.34	2.55	0.36
155.1	2.95	0.32	0.58	0.32	2.37	0.35
195.1	2.77	0.31	0.60	0.31	2.18	0.35
245.1	2.47	0.30	0.45	0.30	2.02	0.32
295.1	2.22	0.24	0.37	0.24	1.86	0.27
395.1	1.89	0.27	0.29	0.272	1.60	0.28
495.1	1.58	0.21	0.25	0.21	1.34	0.23
595.1	1.32	0.24	0.16	0.24	1.17	0.23
795.1	1.06	0.18	0.15	0.18	0.91	0.19
995.1	0.93	0.18	0.16	0.18	0.77	0.17
1495.1	0.67	0.16	0.12	0.16	0.54	0.15
1995.1	0.55	0.16	0.11	0.16	0.43	0.13
2495.1	0.48	0.13	0.09	0.13	0.39	0.12

predicted to quickly dissociate by collisions above the barrier to linearity [26], one must consider the conical intersection with the $\tilde{A}$ state, located 2600 cm^{-1} above the ground state, as the onset of collisional dissociation, as it may occur in the ion source prior to extraction. This threshold of 0.322 eV, above which O_3^+ is subject to large-amplitude motion along the $O_2^+ + O$ dissociation coordinate [14], produces a temperature of 830 K. The actual formation mechanism may further reduce this value.

Present results can be compared with the data of Deng *et al.* [18], also shown in Fig. 2. They have measured the cross section for O^+ production to be at the maximum $(3.5 \pm 0.5) \times 10^{-16}$ cm^2 at 3.75 eV, but only $(1.1 \pm 0.1) \times 10^{-16}$ cm^2 at about 75 eV. The threshold energy is in good agreement with the predicted value of 2.19 eV [24]. The low-energy maximum is in excellent agreement with the present data, but the cross section near 75 eV is more than 3 times lower than the present value. In order to explain this difference, we have plotted in Fig. 2 our results of the apparent $\sigma_m(B_0)$ directly measured cross section, before its correction for the transmission efficiency. The agreement between these cross sections and the data of Deng *et al.* is striking. These authors have not discussed any possible loss of the signal. However, the two experimental setups are of similar scale and the ion-beam energies are the same, suggesting that they should also put forth the question of the transmission efficiency. Thus, we believe the data of Ref. [18] were not corrected for this effect and that may explain the existing difference between the two sets of data.

As already pointed out, for electron energies above the DI threshold, a complex structure of the magnetic-field scans can be seen (Fig. 1). A narrow peak between 110 and 112 mT, the DE signal, is superimposed on a wide DI contribution, which extends between 107 and 115 mT. We first fit the outermost parts of the spectra (from 107 to 110 and from 112 to 115 mT) by a polynomial. The integral of the fit gives the DI cross section and it is used to calculate the transmission factor for the DI process at a given electron energy. These factors are interpolated for all energies above the DI threshold.

Independent DI cross-section measurements are performed for a number of electron energies at a magnetic field of 113.2 mT, where the DE signal is not expected to contribute. These measured cross sections are corrected by the DI transmission factors and absolute DI cross sections are obtained. Finally, the DE cross section is derived by subtracting the DI cross section from the total absolute cross section for O^+ production, for all considered electron energies.

The present results for DE and DI cross sections are shown in Fig. 3. The maximum DE cross section is found to be $(3.4 \pm 0.2) \times 10^{-16}$ cm^2 at 6.1 eV. The threshold energy is estimated to be at (1.5 ± 0.5) eV. The three-body fragmentation DE channel at 7.35 eV [18,24] seems to be less probable and cannot be seen in the present data. The threshold

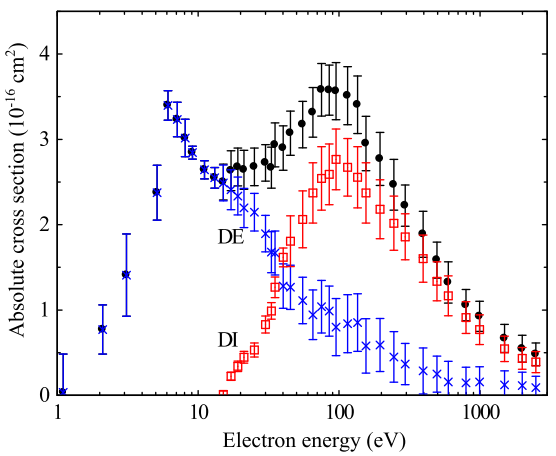

FIG. 3. (Color online) Absolute cross sections for O^+ production versus electron energy: inclusive cross section (closed circles), dissociative excitation (crosses), and dissociative ionization (open squares).

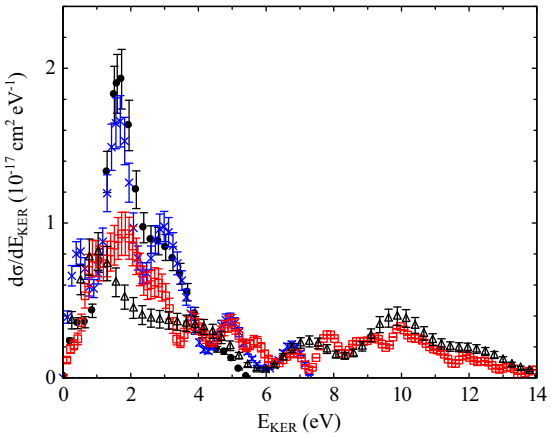

FIG. 4. (Color online) Total kinetic energy release distributions. Electron energies are 15 eV (solid circles), 25 eV (crosses), 95 eV (open squares), and 295 eV (open triangles).

energy for the DI process is found to be at (15.5 ± 0.5) eV and is in agreement with the value of 14.26 eV found in the literature [18,24]. The maximum of the cross section is found to be $(2.8 \pm 0.4) \times 10^{-16}$ cm^2 at 75 eV. A change of slope of the DI cross section can be clearly seen at 23 eV and it might indicate a new DI channel starting at this energy, due to more favorable Franck-Condon overlap with strongly repulsive potential energy surfaces (discussed below). This is slightly higher than the value predicted [18,24] for dissociative ionization to three particles, reaction (4), at 20.97 eV. Individual DE and DI processes of O_3^+ could not be distinguished under the experimental conditions of the experiment by Deng *et al.* [18].

By using magnetic-field scans of the detected signal, distributions (6) of the total kinetic energy released to the fragments are determined at select electron energies. This procedure has been described elsewhere by Lecointre *et al.* [20]. The results are shown in Fig. 4 for electron energies of 15, 25, 95, and 295 eV. The distributions extend up to 14 eV and have two dominant contributions. The first, low-energy one between 0 and 6 eV, with the peak value near 2 eV, is attributed to the DE process. The second one between 6 and 14 eV, with the peak at 10 eV, is due to the DI process. The kinetic energy released by the Coulomb explosion of the molecule may be estimated from the geometry of the ground and first excited potential energy surfaces of O_3^+, which are likely to be populated, i.e., $X\,^2A_1$, with $r_0 = 1.25$ Å and $\theta = 131.5^\circ$, and $\tilde{A}\,^2B_2$, with $r_0 = 1.37$ Å and $\theta = 111.3^\circ$ [14]. When considering the $O^+ + O_2^+$ channel accessed through a vertical transition to O_3^{2+} and assuming that the charge is localized at the center of mass of the fragments, the KER is inversely proportional to the charge separation

$$d = \left[r_0^2 + (r_0/2)^2 - r_0^2 \cos\theta\right]^{1/2} = r_0[5/4 - \cos\theta]^{1/2}. \quad (7)$$

With the parameters above, we derived $\langle E_{\mathrm{KER}} \rangle = 8.3$ eV at the center of the KER distribution attributed to DI. This value of KER added to the threshold for reaction (3) gives 22.6 eV, to be compared to the apparent threshold of 23 eV visible in the DI yield. The range of accessible KER further depends on the stretching and bending motion of O_3^+, which is expected to be extensive due to its formation in microwave-heated plasma, and the actual charge localization upon electron-impact ionization. The latter effect may be accounted for by considering $r_0 < d < 2r_0$, which produces limiting values $5.7 < E_{\mathrm{KER}} < 11.4$ eV. Moreover, a number of individual peaks over the entire energy region are present in all spectra. This indicates the complex movement of the colliding system on the potential surface and may be related to the internal excitation of the molecular fragments. Unfortunately, we cannot identify particular processes or levels giving these peaks. Also, there are no other results to be compared with the present data.

During the present experiments, the electron-impact ionization cross section of O_3^+ resulting in O_3^{2+} was found to be negligible. This finding is in agreement with the conclusion of Deng *et al.* [18]. We believe that the cross sections for single ionization are themselves small. This means that the lifetime of the doubly charged ozone ion O_3^{2+} is sufficiently short and it dissociates before reaching the detector.

Deng *et al.* [18] have also reported the results of electron-impact dissociation of O_3^+ to the O_2^+ fragment. We have measured the cross section for this process only for the electron energy of 100 eV, because of the large background present. The obtained value was very close to the value for the O^+ fragment, about 3.5×10^{-16} cm^2. The result of Deng *et al.* [18] is lower, 1.1×10^{-16} cm^2 only. It seems that in this case they have lost some signal due to incomplete transmission, as pointed out and discussed above for the O^+ case. However, the transmission efficiency for O_2^+ is expected to be higher than for O^+ because of its lower share of velocity in the center-of-mass frame, according to the momentum-conservation law. Thus, its apparent cross section is expected to be higher than for O^+. An additional argument for this statement is that at 100 eV the DI channel dominates and the cross sections for the two observed fragments should be nearly the same, according to reaction (3). This also introduces the question of the importance of the DI process to three particles, reaction (4). Generally, we believe this reaction should be much less probable and can be ignored in this consideration.

We should return our attention to the magnitude of the measured cross section. The maximum of the cross section is 3.6×10^{-16} cm^2 and it has an average value of 3×10^{-16} cm^2 in the energy range from 5 to 500 eV. The large total electron-impact cross section (when combining O^+ and O_2^+ production) makes it an efficient sink of O_3^+ in the presence of electrons over a wide range of collision energies.

IV. CONCLUSION

Absolute cross sections for electron-impact dissociation of O_3^+ ions producing O^+ fragment ions have been measured for energies from threshold up to 2.5 keV using the animated electron-ion crossed-beam technique. Particular attention has been devoted to account for the loss of signal due to its angular divergence after dissociation. The cross section at the maximum was found to be $(3.6 \pm 0.3) \times 10^{-16}$ cm^2 at 75 eV and such large values of the cross section extend down to low energies. The threshold energy was found to be below 2 eV. Contributions from dissociative excitation and dissociative ionization processes were separated and absolute

cross sections for DE and DI were determined over the whole electron energy region considered.

The present results were compared with the results of Deng *et al.* [18]. The two sets of data agree well at low energies, but our cross sections are significantly higher at high energies, more than 3 times at 100 eV. This discrepancy can be explained by some loss of signal in the experiment of Deng *et al.*

By using magnetic-field scans of the detected signal, distributions of the total kinetic energy released to the fragments were determined, at select electron energies. They exhibit an interesting structure and extend up to 14 eV.

In view of the large cross sections measured here, we can raise the question of the importance of electron-impact ozone ion dissociation in the stratosphere, relative to other competitive mechanisms. In particular, it is probably interesting to investigate the role of electrons originating from the solar wind and penetrating the stratosphere along the polar cusp. Whether they are able to contribute to ozone depletion before being fully thermalized is worth clarification.

ACKNOWLEDGMENTS

The authors value the financial support from the IISN under Contract No. 4.4504.10 and the support of the Association Euratom-Belgian State. D.S.B. is grateful for support from Project No. 171016 from the Ministry of Education, Science and Technological Development of the Republic of Serbia. The authors thank the Forschungszentrum Jülich for lending the ECR ion source as well as all the staff members of the IMCN for their assistance in this experiment.

[1] M. Norval, R. M. Lucas, A. P. Cullen, F. R. de Gruijl, J. Longstreth, Y. Takizawa, and J. C. van der Leun, Photochem. Photobiol. Sci. **10**, 199 (2011).

[2] M. J. Molina and F. S. Rowland, Nature (London) **249**, 810 (1974).

[3] J. C. Farman, B. G. Gardiner, and J. D. Shanklin, Nature (London) **315**, 207 (1985).

[4] V. Vaida and J. Simon, Science **268**, 1443 (1995).

[5] J. A. Davies, W. M. Johnstone, N. J. Mason, P. Biggs, and R. P. Wayne, J. Phys. B **26**, L767 (1993).

[6] M. Allan, K. R. Asmis, D. B. Popovic, M. Stepanovic, N. J. Mason, and J. A. Davies, J. Phys. B **29**, 3487 (1996).

[7] C. J. Sweeney and T. W. Shyn, Phys. Rev. A **53**, 1576 (1996).

[8] M. W. Siegel, Int. J. Mass Spectrom. Ion Phys. **44**, 19 (1982).

[9] K. A. Newson, S. M. Lee, S. D. Price, and N. J. Mason, Int. J. Mass Spectrom. Ion Processes **148**, 203 (1995).

[10] Y.-K. Kim, W. Hwang, N. M. Weinberger, M. A. Ali, and M. E. Rudd, J. Chem. Phys. **106**, 1026 (1997).

[11] Y.-K. Kim, K. K. Irikura, M. E. Rudd, M. A. Ali, P. M. Stone, J. Chang, J. S. Coursey, R. A. Dragoset, A. R. Kishore, K. J. Olsen, A. M. Sansonetti, G. G. Wiersma, D. S. Zucker, and M. A. Zucker, NIST Standard Reference Database 107, Electron-Impact Cross Sections for Ionization and Excitation, available at http://www.nist.gov/pml/data/ionization/index.cfm (NIST, Gaithersburg, 2005).

[12] G. de Petris, Mass Spectrom. Rev. **22**, 251 (2003).

[13] D. C. Frost, S. T. Lee, and C. A. McDowell, Chem. Phys. Lett. **24**, 149 (1974); J. M. Dyke, L. Golab, N. Jonathan, A. Morris, and M. Okuda, J. Chem. Soc. Faraday Trans. II **70**, 1828 (1974); C. R. Brundle, Chem. Phys. Lett. **26**, 25 (1974).

[14] S. Willitsch, F. Innocenti, J. M. Dyke, and F. Merkt, J. Chem. Phys. **122**, 024311 (2005).

[15] L. D. Speakman, J. M. Turney, and H. F. Schaefer III, J. Chem. Phys. **128**, 214302 (2008).

[16] V. Zhaunerchyk, W. D. Geppert, M. Larsson, R. D. Thomas, E. Bahati, M. E. Bannister, M. R. Fogle, C. R. Vane, and F. Österdahl, Phys. Rev. Lett. **98**, 223201 (2007).

[17] M. L. Vestal and G. H. Mauclaire, J. Chem. Phys. **67**, 3767 (1977).

[18] S. H. M. Deng, C. R. Vane, M. E. Bannister, and M. Fogle, Phys. Rev. A **82**, 062715 (2010).

[19] E. M. Bahati, J. J. Jureta, D. S. Belic, S. Rachafi, and P. Defrance, J. Phys. B **34**, 1757 (2001).

[20] J. Lecointre, D. S. Belic, H. Cherkani-Hassani, J. J. Jureta, and P. Defrance, J. Phys. B **39**, 3275 (2006).

[21] J. Lecointre, D. S. Belic, J. J. Jureta, R. Janev, and P. Defrance, Eur. Phys. J. D **50**, 265 (2008).

[22] H. Cherkani-Hassani, D. S. Belic, J. Jureta, and P. Defrance, J. Phys. B **39**, 5105 (2006).

[23] J. Lecointre, M. O. Abdellahi El Ghazaly, J. Jureta, D. S. Belic, X. Urbain, and P. Defrance, J. Phys. B **42**, 075201 (2009).

[24] The dissociation limit energies in [18] are estimated from the kinetic energy releases in the dissociative recombination of the ozone cation given by [16] and ionization energies of neutral fragments given by *CRC Handbook of Chemistry and Physics*, 87th ed. (Taylor & Francis, Boca Raton, 2007).

[25] P. Defrance, F. Brouillard, W. Claeys, and G. Van Wassenhove, J. Phys. B **14**, 103 (1981).

[26] I. Kylänpää and T. T. Rantala, J. Chem. Phys. **135**, 104310 (2011).